Australian Meteorological and Oceanographic Journal 64 (2014) 133-147

Downscaling a reanalysis of extremely cold weather in southern New Zealand

John D. Wilson
Department of Earth & Atmospheric Sciences,
University of Alberta, Edmonton, Canada, T6G 2E3

(Manuscript received November 2013, revised April 2014)

In July 1996 southeastern New Zealand experienced a period of extreme cold, and the resulting pattern of tree damage indicated that cold air ponding had been an important factor. To confirm that hypothesis reanalysis fields (2.5° resolution) have been downscaled dynamically using the Weather Research and Forecasting (WRF) mesoscale model, across nested grids to an inner domain covering an area of about 17 km × 17 km with a horizontal resolution of 222 m. So long as vertical resolution is enhanced near ground relative to the default configuration, WRF resolves small scale drainage flows during strongly stable wintertime conditions over this modest topography (peak elevations above sea level ~400 m, and valley-crest amplitudes ~200 m). A twelve hour spinup resulted in marginally stronger drainage flows than did a six hour spinup, and differences between runs with hydrostatic and non-hydrostatic dynamics also were small. From the evidence reviewed, there seems no reason to regard the meteorology behind the 'Big Freeze' as having been categorically unusual.

Introduction

During early July 1996, southern New Zealand (Fig. 1) experienced an interval of extreme winter cold relative to local normals, with minimum temperatures falling well below –5 °C at some lowland, coastal locations and to –15 °C farther inland (see Table 1). Invercargill's minimum temperature of –9.0 °C in July 1996 represents the extreme over the available record at that station (Invercargill Aero, network number I68443, 1905–2012), the mean and standard deviation of the series of annual minima respectively being –4.6 °C and 1.85 °C. The unaccustomed frigidity and persistence of this cold spell, which followed a storm that had covered the region in snow (Fig. 2), caused much damage to vegetation across the region and a degree of inconvenience and discomfort sufficient to earn it local notoriety as the 'Big Freeze.' Wood (1998) documents the death of hundreds of large, ground-feeding birds and reports that smaller, bush-dwelling birds also were affected, while the Insurance Council of New Zealand cites a cost to the insurance industry of NZ$8.1 million[1].

From the pattern of damage to trees (Fig. 3), which has been documented by Terry (1999), Bannister (2003) and Taylor (2012), it is certain that cold air ponding played a role on the local scale (say, 100 – 1000 m): a circumstance that is only to be expected in a hilly region like this. More interestingly, the question arises as to whether a regional-scale 'lake' of cold air was formed (e.g. Mori and Kobayashi 1996), accumulating in the bottoms, deepening day by day, and draining down valleys to the coast. The few available meteorological records in the district shed no light on the matter, and so to that end the weather model WRF-EMS has here been employed to 'downscale' reanalysis fields across a series of nested grids, the finest of which (see Fig. 1) covers an area of about 17 km × 17 km with a horizontal resolution of about 222 m. The centrepoint of this innermost domain lies at (46.1536°S, 169.2794°E), corresponding to the homestead at *Strathearn* in the Wairuna catchment situated between the towns of Gore (in Southland) and Balclutha (in South Otago). From the downscaled fields of surface wind direction and potential temperature θ it will be confirmed that cold air drainage was indeed (according to WRF) a significant influence on the Big Freeze of 1996.

The discussion will focus on early morning conditions (0600 NZST) on 4 July 1996, by which time the cold conditions were well established (note: New Zealand Standard Time NZST=UTC+12). On 4 July the solar declination angle is about 23°N, with the result that at latitude 46°S noon solar elevation is only 21° and the duration of sunlight briefer than nine hours. The fresh snow cover, resulting in a high

[1] This figure (icnz.org.nz/statistics-data/the-cost-of-disaster-events/) is not inflation-adjusted, and it does not reflect (possible) stock losses which (for the most part) are uninsured. That it is unremarkable relative to other weather (and flood) related insurance costs that have occurred in New Zealand may to some extent reflect the low population density of the region.

Corresponding author address: John D. Wilson, Department of Earth & Atmospheric Sciences, University of Alberta, Edmonton, Canada, T6G 2E3. E-mail: jaydee.uu@ualberta.ca

Table 1. Daily minimum and maximum temperatures (at nominally 1.5 m AGL) for the first half of July 1996, from available records nearest to the origin of the computational domain (i.e. closest to *Strathearn*). The stations, whose approximate locations are given on Fig. 1, are: Tapanui (Tap., network number I59921, elevation 180 m ASL, ~23 km from *Strathearn*), Gore AWS (network number I68182, elevation 123 m ASL, ~31 km), Balclutha Finegand (Bal., network number I69273, 6 m ASL, ~38 km) and Invercargill Aero (Inv., network number I68433, ~2 m ASL, ~79 km from *Strathearn*). Recall that NZST=UTC+1200, and that in NZMS files for daily extremes the maxima and minima are registered for 2100 UTC. From the National Climate Database (www.cliflo.niwa.co.nz).

		T_{min}				T_{max}			
Location July normals	**61 – 90,** 71 – 00*	*Tap. 1.3**	*Gore 1.0***	*Bal. 1.0**	*Inv. 1.1**	*Tap. 8.6**	*Gore 8.2***	*Bal. 9.2**	*Inv. 9.6**
30 Jun (UTC)	1 Jul (NZST)	-1.9	-0.2	0.3	0.9	9.1	6.9	8.3	6.3
1 Jul (UTC)	2	-2.9	-5.4	-1.1	-4.0	2	2.4	3.2	3.9
2	3	-13.5	-10.5	-6.3	-8.0	5	1.2	3.5	1.5
3	4	-15.3	-10.5	-6.5	-9.0	-0.6	-2.7	3.1	1.7
4	5		-9.6	-4	-7.3	0.9	-1.0	2.8	1.7
5	6	-10.2	-8.5	-5.5	-7.9	5.2	1.0	8.4	2.6
6	7		-9.8	-6.2	-7.6		-0.9	3.2	1.8
7	8	-11.7	-8.6	-6.3	-9.0	3.5	-1.0	3.8	2.8
8	9		-9.0	-6.2	-7.6	3.5	2.2	7.1	4.3
9	10	-10.2	-6.7	-1.3	-7.0	4.1	1.2	7.9	4.4
10	11	-1.2	-0.9	1.7	-0.3	7.9	3.2	8.7	6.9
11	12	-3.4	-2.9	-1.0	-3.9	5.9	3.8	6.6	6.6
12	13	-9.0	-4.0	-3.5	-5.0	7.2	4.4	6.4	6
13	14	-8.2	-4.0	-3.2	-4.9	3.2	0.9	3.0	4.3
14	15	-2.0	0.5	-1.6	0.0	7.5	6.1	5.8	7.9
15 Jul	16 Jul	3.7	2.9	-3.0	2.8	7.6	5.4	7.1	6.9

Table 2. Daily 0600 NZST wind direction (deg.) and speed (m s^{-1}) at Gore (46.115°, 168.887°, 123 m ASL) and Nugget Point (46.449°, 168.81°, 129 m ASL) automatic weather stations (AWS). Nugget Point is a coastal station on the promontory defining the southern end of Molyneux Bay. From the National Climate Database (www.cliflo.niwa.co.nz).

		Dir.	*Spd.*	*Dir.*	*Spd.*
Location		*Gore*		*Nugget Pt.*	
30 Jun (UTC)	1 Jul (NZST)	280	3.1		
1 Jul (UTC)	2				
2	3	50	2.6	310	3.6
3	4	0	0.8		
4	5	30	4.6	350	6.2
5	6	60	2.6	20	7.2
6	7	40	1.5		
7	8	50	2.6	50	1.5
8	9	70	1	40	16.5
9	10	30	3.1		
10	11	60	1.5		
11	12	80	0.5	160	2.1
12	13			100	3.6
13	14			360	2.1
14	15	90	5.1		
15 Jul	16 Jul	80	8.2	50	21.1

Fig. 1. Partial view of terrain of Southland and South Otago, New Zealand, identifying locations referred to in the text. Inset outlines New Zealand (North Island, South Island and, southernmost, Stewart Island), and the rectangle at the base of the South Island indicates the outermost domain (domain 1) for downscaling simulations (the city of Invercargill is located at the tip of the arrow). The + identifies the centre of all three computational domains, that centre being co-located with the *Strathearn* homestead south of State Highway 1. The dashed line identifies the boundary of domain 2 (57 km × 57 km) and the dotted line the boundary of domain 3 (innermost, 17 km × 17 km). This study will focus on conditions in the Wairuna valley near *Strathearn* (+); the valley, running between Gore and Clinton, is defined by the Blue Mountains (top centre) and the Kaihiku Range (running WNW–ESE across the centre). The town of Gore is pinched between hills at the head of the broadening valley that exits (not shown) to a coastal plain at the lower left. The Clutha (Mata-Au) River runs south through the upper-right quadrant of domain 2 (dashed rectangle), through Balclutha, and emerges at Molyneux Bay. For more detail please visit www.nztopomaps.com.

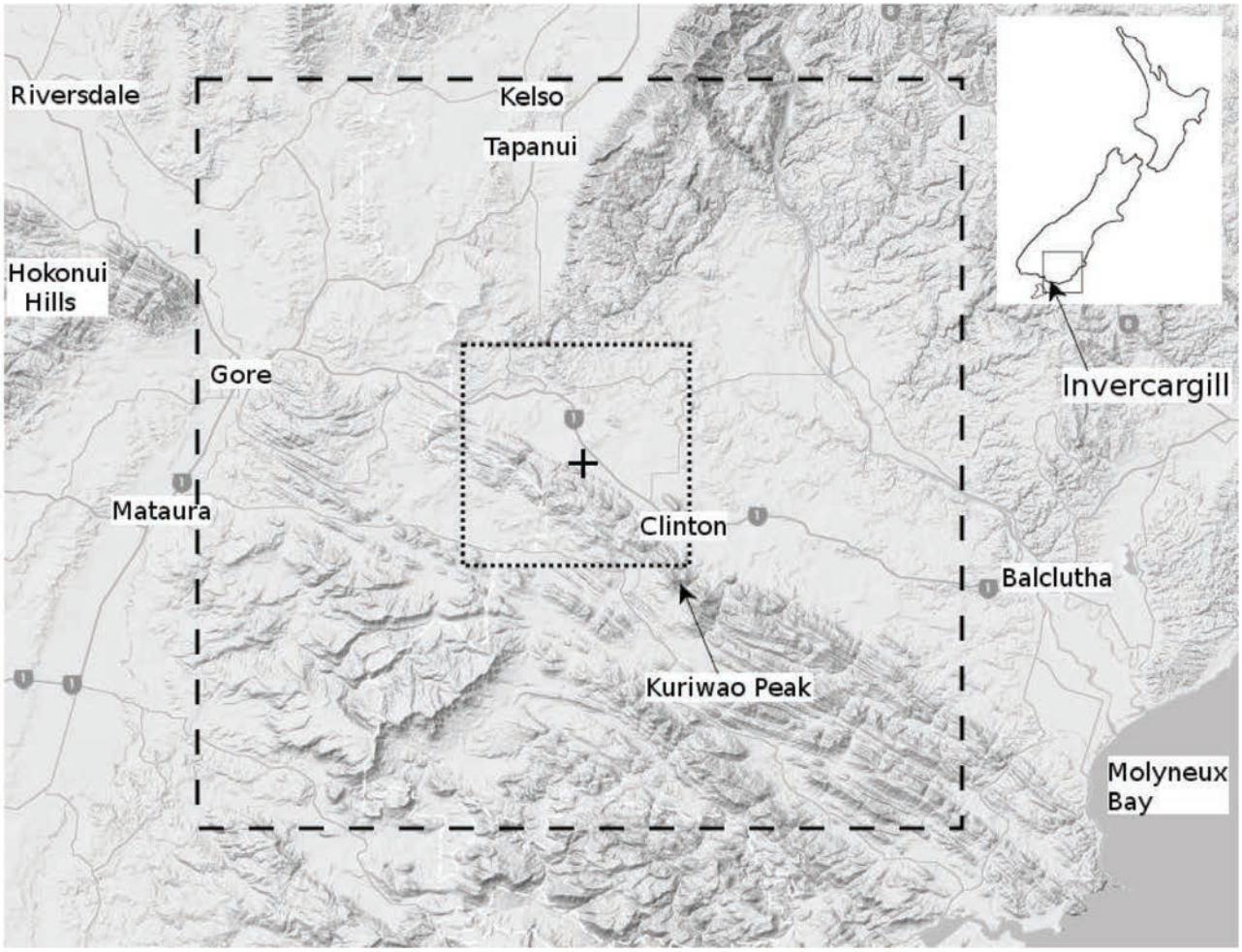

solar reflectivity (albedo), must further have reduced net solar radiative heating. Given also that little or no large scale temperature advection was occurring (see Section 2), conditions certainly were favourable for the cold to persist (albeit with the daytime amelioration evidenced by Table 1) and for the development of regional scale drainage flows. Figure (1) suggests cold air sliding off the slopes would drain down the low land along the Clutha (or Mata-Au) River to Molyneux Bay, and/or along the Mataura River towards coastal Southland.

Section 2 will review the synoptic scale conditions preceding and during the cold spell, as represented by NCEP (National Center for Environmental Prediction) reanalyses. Section 3 will give some background on the 'downscaling' of weather data, and on the WRF model. Section 4 gives meteorological fields in the focal region as downscaled by WRF, using 12 hour forward time integrations to 0600 NZST 4 July 1996. Conclusions are presented in Section 5.

Synoptic scale conditions preceding and during the Big Freeze

Invercargill Aero weather station reported snow as of 1996-06-30 (UTC) at 11:59 UTC, but (as NZST=UTC+12) this should be interpreted as snow on 1 July. This was the only day registering snowfall at Invercargill over the period of 20 June – 20 July, and discussion at www.weatherforum.org.nz

Fig. 2. A view looking south towards the Hokonui Hills on 9 July 1996 (taken near Riversdale, by Lois Shallard).

gives 1 July as the date of snowfall over most of Southland[2]. Hail and lightning were also associated with the storm, whose passing is conveyed by Figs 4(a)–(d) from the NCEP re-analysis covering 1200 NZST 30 June to 0600 NZST 1 July. The tight isobar spacing is of course indicative of strong winds in southern New Zealand. At 0600 NZST 1 July (Fig. 4(d)) a trough (slight kink in surface isobars) runs just south of southern New Zealand (through Stewart Island) and extends eastward to the low pressure system. One might surmise a cold front would have lain along this trough just offshore (south) of the South Island, and indeed the New Zealand Meteorological Service (NZMS) forecast for noon that day (1200 NZST 1 July, Fig. 5(a)) indicated a cold front about to advance northward onto the extreme south of the South Island. Thus the NCEP DOE II reanalysis is consistent with the original NZMS short range forecast.

The 850 hPa re-analysis at 0600 NZST 1 July (Fig. 6) implies a SW geostrophic flow aloft advecting colder air over southern NZ, and if the isotherm packing is insufficient to suggest a cold front one must recall the relatively low resolution of the re-analysis (2.5°) and the sparsity of radiosonde stations over the southern ocean. Farther aloft at the 700 hPa level a region of synoptic scale ascent (vertical velocity expressed in the isobaric coordinate system $\omega \sim -0.1$ Pa s^{-1}) covered the bottom of the South Island (not shown).

Taylor's (2012) booklet speaks of a 'big freeze that immediately followed a week of stormy conditions,' conditions that had culminated 'with a day of driving snow that left a cover of 12 to 15 cm (and much more in drifts) over a lot of Southland, West Otago and most of South Otago.' The wide snow coverage is consistent with the ECMWF interim reanalysis (depth of water equivalent; not shown) which, as of 1800 UTC 3 July, indicated snow coverage over most of the South Island.

In the wake of this storm that had delivered a deep cover of snow, a strong anticyclone developed over the area. The

[2] Terry (1999) states 'The snowfalls that marked the commencement of the Big Freeze began on Sunday evening, 30th June, and continued intermittently until early on Tuesday morning, 2nd July.'

Fig. 3. A view looking southeast from Old Lake Road in eastern Wairuna, showing a frost-damaged cabbage tree (*Cordyline australis*) nine months after the Big Freeze. The hill on the right of the tree is Kuriwao Peak (639 m, latitude 46.233S, longitude 169.367E) on the Kaihiku Range. (Courtesy of H. Taylor.)

surface expression of this high, as of 0600 NZST on 4 July, is shown by Fig. 7, with the sea level pressure exceeding 1040 hPa (a figure that concurs with the short range NZMS forecast at the time, Fig. 5(b)). The corresponding 850 hPa height and temperature fields (Fig. 8) indicate the weak regional-scale height gradient (implying light winds aloft) and the relatively homogeneous temperature: under these circumstances the contribution of thermal advection to the daily temperature cycle must have been unimportant. At the 700 hPa level, subsidence was occuring over the South Island ($\omega \approx 0.15$ Pa s^{-1}, not shown). Such conditions, especially given the fresh snow cover and short mid-winter days, should have resulted in cold air drainage off the slopes and ponding in the valleys. Terry (1999) notes that 'Southland's weather for this period was characterised by clear, sunny skies and a distinct absence of wind.' Bannister (2003) describes the frost as 'intense, persistent, and all-pervasive.' Table 1 gives the daily minimum and maximum temperatures at available stations, in comparison with the July normals.

The cold spell lasted (broadly) to about 14 July. Fig. 9 gives the ten-day time-averaged anomaly (1–10 July) in the height of the 700 hPa surface. At the 700 hPa level the centre of the high was located south of NZ, and the mean magnitude of the 700 hPa height anomaly, averaged 1–10 July, exceeded 13.5 dam (relative to 1981-2010 normal). The sea-level pressure anomaly, again averaged from 1–10 July, exceeded 15 hPa (see Fig. 10). Winds aloft were light, e.g. the mean speed at 850 hPa during 1–10 July over southern New Zealand was lighter than 4 m s^{-1}, suggesting that the main driver for temperature evolution during this period would have been the daily cycle in net radiation and the (concomitant) sensible heat exchange between atmosphere and surface. The 850 hPa temperature field, averaged for 1–10 July 1996, showed only a weak (~ –2 °C) cold anomaly, which (furthermore) was centred well north of Otago and Southland (not shown); and the July 1996 mean temperature anomaly at 850 hPa reported

Fig. 4. Evolution of sea-level corrected surface pressure [hPa] during the storm that preceded the cold spell. (NCEP Reanalysis II.)

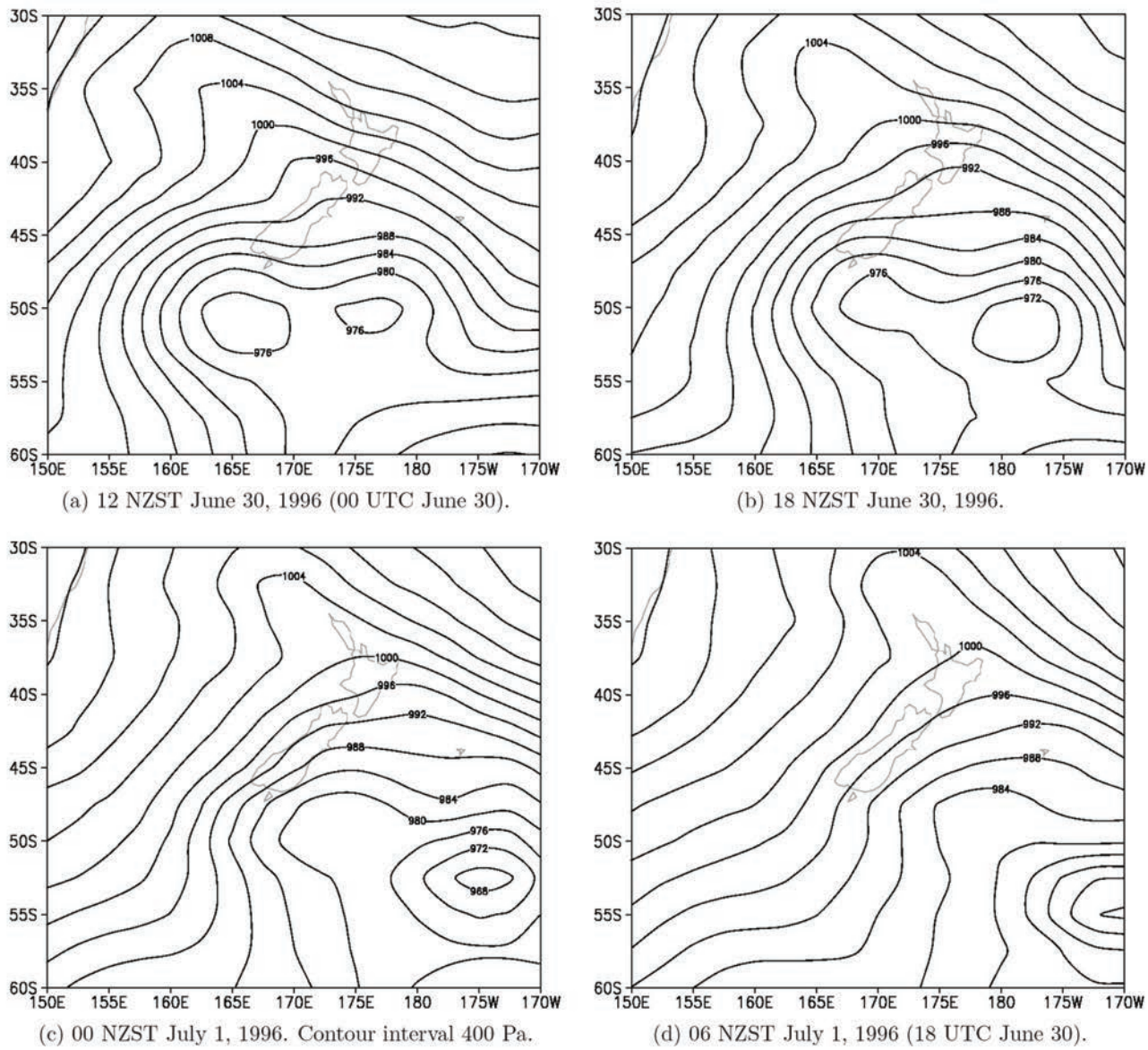

(a) 12 NZST June 30, 1996 (00 UTC June 30).

(b) 18 NZST June 30, 1996.

(c) 00 NZST July 1, 1996. Contour interval 400 Pa.

(d) 06 NZST July 1, 1996 (18 UTC June 30).

by the Invercargill radiosonde station[3] was +1.2 °C (relative to the 1966–95 normal), the standard deviation of the July monthly anomaly (over 1958–2012) being 1.1 °C. Thus there was no sustained cold anomaly in the temperature aloft (at 850 hPa) over Southland. However Fig. 11 shows that when the 850 hPa temperature is averaged over a shorter interval (29 June–2 July 1996), a marked cold core (< –5 °C relative to normal) was centred over southern New Zealand. Thus in terms of causality, it can be said that the low surface temperatures that were experienced reflect an incursion of cold air (delivered by the storm) arriving in mid-winter over (and in association with) fresh snow cover, followed by prolonged calm, clear conditions that were conducive to strong overnight cooling.

To put this event in perspective, the New Zealand Official Yearbook states of 1996 that 'the lowest temperature for the year was –15.3 °C, recorded at Tapanui, Southland on 4 July, the same day as lowest ever minimum air temperatures were recorded at both Gore (–10.5 °C) and Invercargill (–9.0 °C).' According to Emergency Management Southland (www.civildefence.co.nz) 'Snow in July 1996 was followed by ten consecutive frosts and was labelled the 'big freeze' and caused many frozen/burst pipes and tree deaths. The –14.2 °C frost on the 3 July 1996 was the coldest on record since 1910' (unfortunately the location and time of this measurement is not given, but the degree of cold is certainly compatible with the data of Table 1). As already noted the

[3] Abstracted from the Met Office Hadley Centre observations dataset 'hadat2 monthly stations.txt' available at hadobs.metoffice.com/hadat/hadat2.html.

Fig. 5. NZ Meteorological Service short range forecasts valid 1200 NZST, as published ('Noon forecast') in the Otago Daily Times (scanned copies provided by Dunedin Public Library have been edited by the author to improve clarity). (a) the storm that preceded the July 1996 'Big Freeze', delivering a blanket of snow; and (b) the subsequent anticyclone. Isobar spacing is five hPa; the innermost (and unlabelled) isobar of the cyclone as of 1 July is the 965 hPa contour. (See Fig. 1.2 of Terry 1999 for a sequence of these charts spanning 29th June–17th July.)

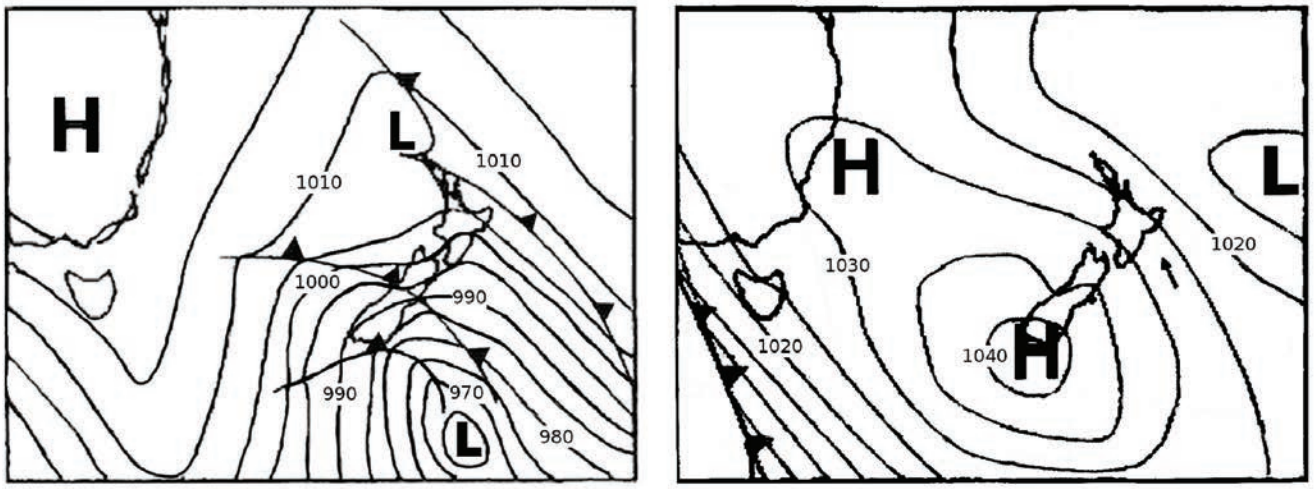

(a) Fcst for 12 NZST July 1, 1996 (00 UTC July 1). (b) Fcst for 12 NZST July 4, 1996.

minimum temperature of –9.0 °C in July 1996 represents Invercargill's record minimum temperature over the period of record (1905–2012). Though no comparable duration of record exists for any other fixed location in the region of interest, it is not unreasonable to conclude that on the 100–yr time scale, the 1996 cold spell was indeed extreme.[4]

Downscaling a reanalysis using WRF

Dynamical downscaling can reveal weather (or climate) detail on a fine spatial scale, given the conditions on a much coarser scale; low resolution initial and boundary conditions, usually stemming from an analysis or reanalysis, can be used to 'drive' a numerical weather prediction model running on a high resolution grid, such that the solution comes into equilibrium with the provided large scale fields. Thereby solutions are obtained that satisfy the equations of motion and other constraints, while reflecting those features (unresolvable by the reanalysis) that owe to influences such as topography, or spatially-varying surface heating/cooling, and so forth. Of course arbitrary choices must be made, e.g. which reanalysis to use as a starting point; weather model dynamics and physics (parameterisations); the model configuration (domain, horizontal resolution, one-way or

Fig. 6. 850 hPa height contours (solid, six dam interval) and isotherms (2 K interval) at 1800 UTC 30 June (0600 NZST 1 July, 1996). NCEP/DOE AMIP-II Reanalysis.

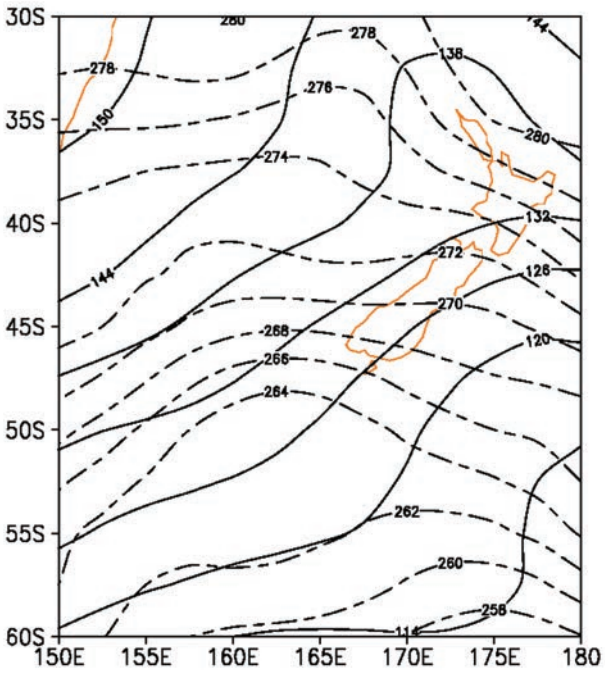

two-way interaction of nested grids); vertical resolution; and the duration of the downscaling integration (known as 'spin-up' time). These choices are detailed below.

Several studies have refined or tested the capability of the Weather Research and Forecasting Model (WRF–ARW) to resolve boundary layer and surface state, over relatively level terrain (e.g. Shin and Hong 2011), over ocean (e.g. Suselj and Sood 2010) or (of particular interest here) over variable terrain. Focusing on the performance of WRF–

[4] This begs some qualification, for perception of what constitutes 'extreme' weather varies according to whether the criteria are strictly meteorological, or relate to one or another of weather's impacts. After 'five days of sustained storms' in September 2010 – i.e. spring, and therefore lambing time—a Federated Farmers adverse events spokesman (Southland farmer D. Rose) stated: 'the spring storm of 2010 is frankly the worst in a generation... The last big dump of snow we had was 14 years ago in the winter of 1996, while the last time we had anything this severe was 38 years ago, in 1972' (ONE News/New Zealand Press Association, September 22, 2010). Decades earlier, during 1939, snow falls of up to 2 m occurred between Gore and Balclutha. Evidently then however cold, the 1996 Big Freeze was not extreme in terms of snow depth or stock losses.

Fig. 7. Sea-level corrected surface pressure [hPa] at 00 UTC 3 July (0600 NZST 4 July, 1996). NCEP/DOE AMIP-II Reanalysis.

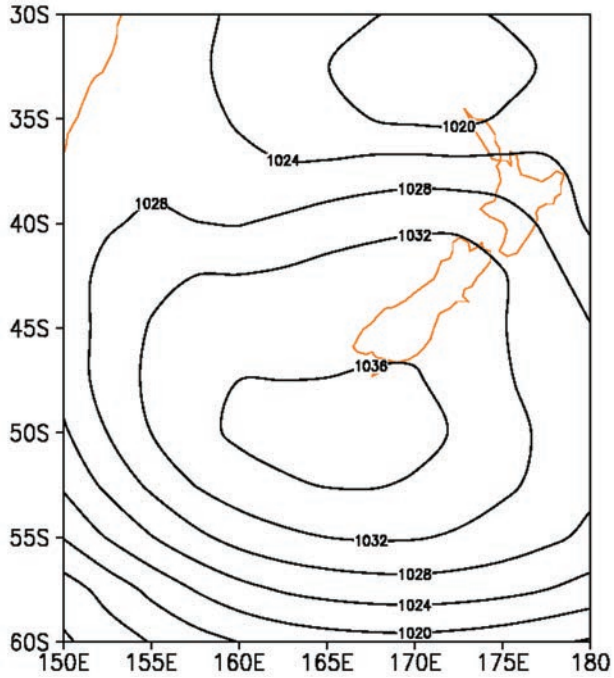

Fig. 8. 850 hPa height contours (solid, 6 dam interval) and isotherms (2 K interval) at 1800 UTC 3 July (0600 NZST 4 July, 1996). NCEP/DOE AMIP-II Reanalysis.

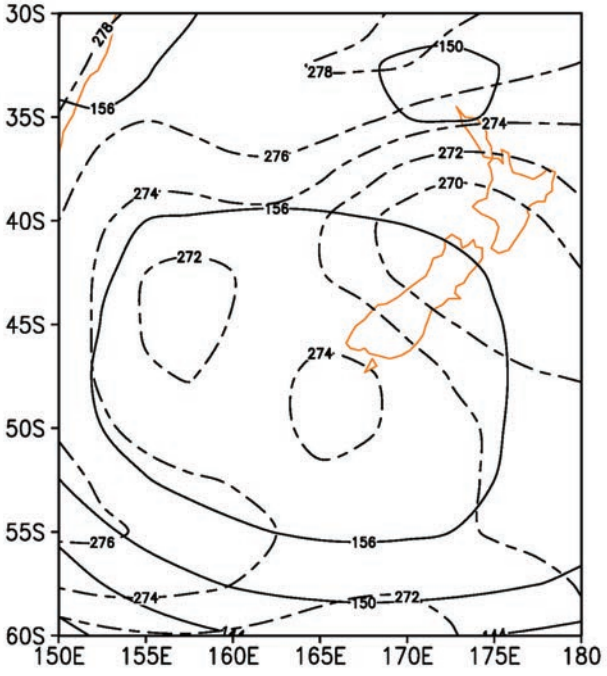

Fig. 9. Mean deviation (m) of 700 hPa height, averaged 1-10 July 1996, from the 1981–2010 normal for July. At the centre of the anticyclone, ten-day mean heights exceed normal by more than 13.5 dam. The implied upper wind anomaly over southern New Zealand is an easterly. (NCEP reanalysis.)

Fig. 10. Mean deviation of surface pressure [hPa], averaged 1-10 July 1996, from the 1981-2010 normal for July. At the centre of the anticyclone, 10-day mean pressures exceed normal by more than 15 hPa. Allowing for friction-induced cross- isobar flow, the implied surface wind anomaly over southern New Zealand is a south-easterly. (NCEP re-analysis.)

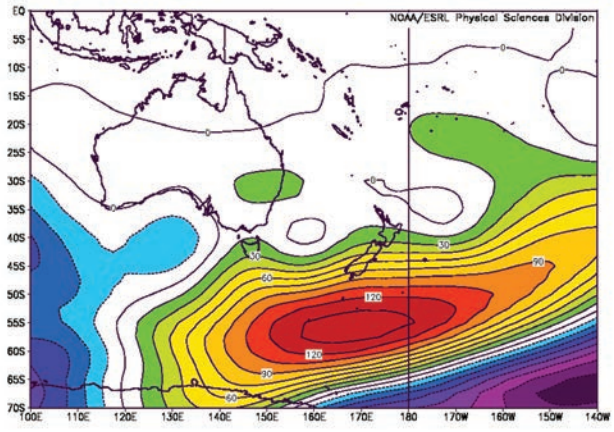

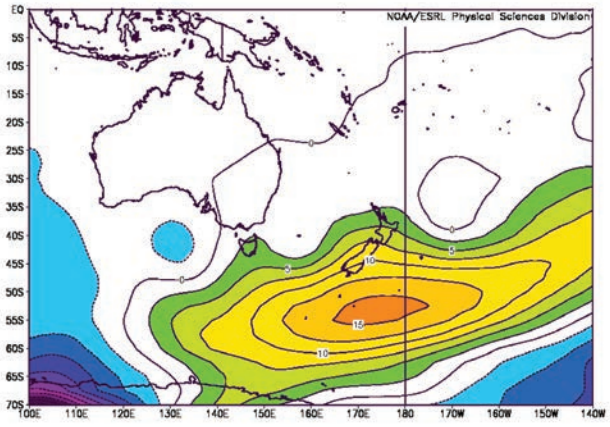

ARW with each of its several available boundary layer parameterisations, Shin and Hong (2011) downscaled NCEP analyses for comparison with measured surface variables and radiosonde profiles for a single day of the CASES 99 field campaign, configuring WRF–ARW with 28 vertical levels and three domains (the innermost covering 3 km × 3 km) linked by one-way (coarse grid → fine grid) interaction. These authors noted 'the representation of surface variables is still uncertain even with state-of-the-art PBL schemes,' a point that, while not surprising, speaks to the non-uniqueness of solutions such as those provided in Section 4. In any case a reanalysis is not useless merely because it is imperfect (i.e. non-unique—and differing from observations, if and where available). Rogers et al. (2013), running WRF–ARW on one-way nested grids (with grid spacings of 36 km, 12 km and 4 km) over the Central Valley of California, observed realistic mesoscale slope flows. Jiménez and Dudhia (2012, 2013) tested WRF's

Fig. 11. Mean deviation of temperature on the 850 hPa surface, averaged 29 Jun-2 July 1996, from the 1981-2010 normal for July. (NCEP re-analysis.)

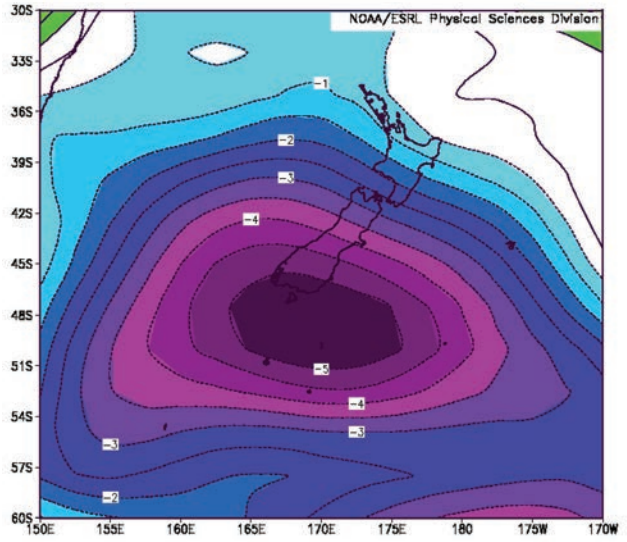

simulation of surface winds over complex terrain (31 model levels; resolution of finest nested grid 2 km; two-way interaction), and reported a refinement whose effect was to roughly to halve the mean absolute error in surface wind speed relative to observations in a region of strong winds (see also Santos-Alamillos et al. 2013). Yang et al. (2013) evaluated the performance of several of the WRF boundary layer parameterisations relative to the quality of prediction of wind speed at typical wind turbine hub heights, running the model with 55 levels and a 12h spinup time with the finest nested grid having a resolution of 1.3 km; in a statement that resonates with those of Shin and Hong (2011) they reported that 'no single PBL parameterisation is clearly superior to the others when all atmospheric conditions are considered.'

a. Provisional capability of WRF to resolve drainage winds

In this section, consider surface layer flow in the vicinity of an infinitely-long ridge oriented along the y-axis. For the purpose of discussion it is convenient (Mahrt 1982) to express the governing equations in a rotated frame of reference whose axes (x, z) are respectively parallel and perpendicular to the surface, which for simplicity (here) is assumed to have constant slope α. Then under the Boussinesq approximation, assuming steady state and neglecting viscous and Coriolis terms, the mean velocity field is governed by

$$\overline{u}\,\frac{\partial \overline{u}}{\partial x} + \overline{w}\,\frac{\partial \overline{u}}{\partial z} = \frac{-1}{\rho_0}\,\frac{\partial \overline{p}}{\partial x} + g\sin\alpha\,\frac{\overline{\theta}}{\theta_0} - \frac{\partial \overline{u'^2}}{\partial x} - \frac{\partial \overline{u'w'}}{\partial z}, \quad \ldots(1)$$

$$\overline{u}\,\frac{\partial \overline{w}}{\partial x} + \overline{w}\,\frac{\partial \overline{w}}{\partial z} = \frac{-1}{\rho_0}\,\frac{\partial \overline{p}}{\partial z} + g\cos\alpha\,\frac{\overline{\theta}}{\theta_0} - \frac{\partial \overline{u'w'}}{\partial x} - \frac{\partial \overline{w'^2}}{\partial z}, \quad \ldots(2)$$

while the thermodynamic equation is

$$\overline{u}\,\frac{\partial \overline{\theta}}{\partial x} + \overline{w}\,\frac{\partial \overline{\theta}}{\partial z} = -\frac{\partial \overline{u'\theta'}}{\partial x} - \frac{\partial \overline{w'\theta'}}{\partial z}. \quad \ldots(3)$$

Fig. 12. Transect of surface elevation across the valley at Wairuna. The transect is at constant longitude 169.274E, and runs through *Strathearn* at latitude –46.154°. The latitude axis, spanning domain 2 of the WRF simulations, covers a distance of 42 km (88 × 0.00427°). The Wairuna valley (at the centre of the diagram) is defined by the Kaihiku Range at the south (left) and the Blue Mountains to the north (right).

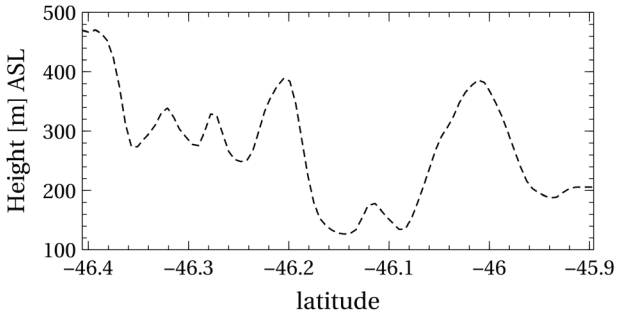

Here $\overline{u}$ is the mean downslope velocity component; $\overline{w}$ is the mean velocity component normal to the surface; $\overline{p}$ is the mean pressure departure from a hydrostatic and adiabatic reference state; $\rho_0 = \rho_0(z)$ and θ_0 = const. are the density and (constant) potential temperature of the reference state; $\overline{\theta}$ is the mean deviation of the potential temperature from the reference state; and terms involving velocity fluctuations correspond to turbulent (i.e. unresolved) transport ($\overline{u'w'}$ and $\overline{w'\theta'}$ in particular being the eddy fluxes of downslope momentum and of sensible heat normal to the sloping surface). Notice that if $\alpha < 0$ and $\overline{\theta} < 0$ the contribution of buoyancy is such as to accelerate $\overline{u}$ (cold air accelerates down slope).

One may assume that the radiation scheme in WRF (in combination with the land surface specification) must result in a plausible daily cycle in net radiation at the surface, such that the local surface sensible heat flux density Q_{H0} extracts heat from the base of the atmosphere overnight (nocturnal surface inversion). Correct vertical redistribution (mixing) of the resulting temperature deficit hinges on the quality of the turbulence parameterisation and vertical resolution (addressed below), but clearly on non-level terrain the extraction of heat from the surface layer must result in alongslope buoyancy forces, that 'drive' drainage winds. As a non-hydrostatic model, and with provisos as to the adequacy of the resolution, we may assume WRF is capable of properly representing not only the advection terms of the left hand sides of Eqns. 1–3 but also the buoyancy terms resulting from inhomogeneity of the field of mean potential temperature. Regarding the suitability of WRF to capture drainage winds there remains only the question of the adequacy of its means of representing divergences of the turbulent (momentum and heat) flux densities, an adequacy which depends on the choice of turbulence closure scheme (PBL and surface layer schemes), and on provision of adequate vertical resolution.

b. Selection of Parameterisation Schemes

Default schemes for shortwave radiation (Dudhia scheme) and longwave radiation (Rapid Radiative Transfer Model) were specified, while given the meteorological regime (intensely stable stratification) it was appropriate to turn off the convection (cumulus) parameterisation. Comparative runs with and without optional topographic effects on solar radiation (shading) and drag on unresolved (subgrid) terrain suggested there was no advantage (in this case of very moderate terrain) to their inclusion.

Potentially the most important of the choices to be made in configuring WRF for this study was the manner of representing unresolved turbulent vertical transport ('mixing') in the planetary boundary layer (PBL), and simulations reported here used the default 'YSU' (Yonsei University) scheme. This is a development of the Troen and Mahrt (1986) '*K*–profile scheme' that had been intended 'for applications where high vertical resolution is not possible' such that it is envisaged as coming into play above the surface layer. The latter, assumed to be in equilibrium and to extend to a height of one tenth of the boundary layer depth, is envisaged as not necessarily being resolved, though that is not to say that it will be incorrect or inappropriate to use YSU if (as here) one is running WRF with gridpoints in the surface layer. Assuring a plausible closure within the surface layer is a concern here in that the surface layer hosts (i.e. is the domain of) the shallow drainage winds of interest.

Taking the case of the unresolved (turbulent) momentum flux, the closure is (Noh et al. 2003, Eqn. 36; Shin and Hong 2011, Eqn. 2)

$$\overline{u'w'} = -K_m \left(\frac{\partial \overline{u}}{\partial z} - \gamma_m \right) + \left(\overline{u'w'}\right)_\delta \left(\frac{z}{\delta}\right)^3 \qquad ...(4)$$

where δ (loosely, boundary layer depth) is to be interpreted as the height of the minimum heat flux, $K_m(z)$ is the profile of the eddy viscosity, and γ_m (zero in the stable case, as here) is a threshold value of the wind shear such that a countergradient momentum flux may be parameterised. The term in $\overline{u'w'}_\delta$ represents entrainment of momentum across the top of the ABL. The profile of eddy viscosity used in the YSU scheme is a refinement of

$$K_m = \frac{k_v u_* z}{\varphi_m \left(z/L\right)} \left(1 - \frac{z}{\delta}\right)^p \qquad ...(5)$$

(Brost and Wyngaard 1978; Troen and Mahrt 1986) where k_v is the von Karman constant, u_* is the friction velocity, $\varphi_m(z/L)$ is the universal Monin-Obukhov function for the normalised mean wind shear, and L is the Obukhov length. Eqn. 5 features the standard (Monin-Obukhov) eddy viscosity profile of an equilibrium surface layer, attenuated arbitrarily above the surface layer so as to vanish at $z = \delta$ (following Troen and Mahrt, for simplicity $p = 2$).

Default schemes for the surface layer (Monin-Obukhov) and land surface (NOAA Land Surface Model) were used, their joint function being to provide surface fluxes having the correct relationship to conditions at the lowest model gridpoint (the fluxes are calculated using bulk transfer formulae whose coefficients are tuned to Monin-Obukhov similarity theory). In summary, this simple eddy-viscosity formulation of the boundary layer and its coupling to the surface should be adequate for the application at hand: computation of the turbulent momentum and heat flux divergences across a wintertime boundary layer, and in particular within the shallow drainage layer adjacent to ground.

c. Vertical resolution

Turning now to the issue of resolution, let $\overline{u}_P$ represent the alongslope component at the gridpoints P nearest to ground. In numerical models of turbulent flow, momentum loss from the lowest layer of control volumes (encompassing P) to the underlying terrain is parameterised by adopting an assumed (semi-logarithmic) profile of mean windspeed extending below P, a relationship that (in effect) determines the surface drag ($\rho_0 u_*^2$) given (z_P , z_0 , $\overline{u}_P$, L), where z_P is the height of this lowest gridpoint above ground and z_0 is the surface roughness length. The key to properly treating the drainage layer will be to require that the lowest gridpoint is sufficiently close to ground to legitimize that assumption, and that the transverse grid spacing Δz is fine enough to resolve the profiles of the drainage layer.

In the default scenario for vertical resolution (45 levels, automatically distributed), at the gridpoint nearest to *Strathearn* (where surface elevation is 126.9 m ASL) the first three 'hybrid levels' of WRF–EMS simulations fall at heights AGL of 26.8, 92.4 and 182.4 m. To provide better resolution of the surface layer (and slope winds), simulations reported here used a total of 59 levels spanning from the surface ($p = p_0$) to the 50 hPa (p_T) level, with the lowest 18 of these uniformly ($\Delta\sigma = 0.002$) spanning $1 \geq \sigma \geq 0.966$ (the grid interval was gradually increased above $\sigma = 0.966$). Note that with $\Delta\sigma = 0.002$ near ground, the height resolution $\Delta z \sim (p_0 - p_T)\,\Delta\sigma/(\rho_0 g) \sim 15$ m. These σ levels resulted in the lowest three levels at the gridpoint nearest to *Strathearn* falling at 7.6, 22.9 and 38.2 m AGL. Simulations with finer resolution (e.g. $\Delta\sigma = 0.0015$ or 0.001) were attempted, but were unsuccessful.

d. Other details of the WRF simulations

Simulations were performed using the ARW dynamical core (National Center for Atmospheric Research Advanced Research dynamics solver) in non-hydrostatic mode on a Lambert conformal grid. All results reported in this paper stem from using the NCEP II reanalyses (horizontal resolution 2.5° or about 278 km) for initial and boundary conditions (the ECMWF ERA reanalysis resulted in stronger overall winds, and a consequently less definitive pattern of nocturnal slope winds). A twelve hour integration is considered sufficient spinup time (Yang et al. 2013; WRF User's Page www.mmm.ucar.edu/wrf/users/), and differences with respect to shorter 6 h integrations ending at the same valid time (0600 NZST 4 July 1996) were small. The time step, selected automatically

to satisfy the Courant condition, was 10 s.

The outermost domain (167.986–170.547°E, 47.0352–45.2715°S) contained 100 × 100 columns of gridpoints with a nominal horizontal gridlength Δ_1 = 2 km, and covered an area of 200 km × 200 km centred (arbitrarily) on the coordinates (46.153645°S, 169.279410°E) of the homestead at *Strathearn* (designated + on Fig. 1). *Strathearn* is situated at the flank of a valley just north of the slope leading up to Stony Peak on the Kaihiku Range, and a view of the terrain on a constant longitude transect through *Strathearn* is given by Fig. 12. Nested domains, centred near the same point, had gridlengths $\Delta_2 = \Delta_1/3$, $\Delta_3 = \Delta_2/3 = \Delta_1/9$ (etc). Domain two (168.905–169.653°E, 46.4116–45.8962°S) covered about 57 km × 57 km (88 × 88 gridpoints, spacing 667 m) while the innermost domain (169.172–169.385°E, 46.2281–46.0807°S) covered about 17 km × 17 km (76 × 76 gridpoints, spacing 222 m). The simulations use one-way interaction (i.e. no feedback of the flow on the nested grid back onto the larger scale).

Results of WRF downscaling simulations

The following results are from a 12 h, non-hydrostatic simulation initialised (time t_0) with NCEP II reanalysis fields for 1200 UTC on 3 July 1996. Thus the output fields to be shown are valid at t_0 + 12 h, i.e. 1800 UTC 3 July, or 0600 NZST 4 July.

a. Wind field

Figure 13 shows the wind field at 850 hPa over SE New Zealand at 06 NZST on July 4, the light SSE or SE wind being consistent with the 850 hPa height field of the reanalysis (Fig. 8). Notice the penetration of the 850 hPa wind inland over Molyneux Bay and the lowland of interest. Fig. 14, giving the corresponding low level (10 m) wind field, indicates that the latter does not penetrate inland from the coast, but rather, a firm (2–4 m s^{-1}) southerly onshore breeze converges near the coast at Molyneux Bay with a north-westerly (downvalley) surface wind over the Clutha River delta. Comparable simulations based on other reanalyses placed the convergence zone further offshore or further inland, but shared the same overall pattern. During the Big Freeze, early morning (0900 NZST) winds at the Gore AWS (Table 2), located at (46.115°, 168.887°) within the (conjectured) SSW-NNE oriented drainage corridor, were mostly light northeasterlies (thus, compatible with the suggested pattern of surface flow); on July 4 (specifically) the wind was reported as a 0.3 m s^{-1} northerly[5].

Figure 15 shows the 10 m wind vectors over domain two. Cross-contour (downslope) winds are evident on almost all terrain features, e.g. on the Blue Mountains (top centre) and on the slope south of *Strathearn* (note: the diagram is centred near *Strathearn*), and in the Clinton valley at the lower right of the figure we see the formation of the downvalley drainage flow that emerges to the coast at Molyneux Bay. Figure 16 differences this low level wind field against that stemming from a simulation that in every respect was identical, except that it used the default 45 vertical levels. The difference field represents a strengthened downslope component, and indicates that the provision of finer vertical resolution near ground has emphasised (presumably, better represented) the gravity driven component that is hypothesised to have been present.

Figure 17 gives the 10 m wind field over domain 3, indicating no qualitative difference relative to domain 2. Notice that at around 169.26°E and in the latitude range 46.19°–46.16°S the topographic contours run more or less east-west, and the 10 m wind, a southerly, is directed downslope. Figure 18 plots a transect of vertical profiles of the downslope component $\overline{v(z)}$ at multiple points along the slope in this subregion. The downslope wind layer deepens with increasing distance from the ridge, and the peak downslope velocity, occurring at the gridpoint (σ = 0.998) closest to ground[6], likewise increases to a maximum value of $\overline{v}$ = –2 m s^{-1} slightly upwind of the valley floor. Surface wind decays as the valley floor is reached, with a suggestion that the drainage layer runs over the top of the surface air in the valley (c.f. Mori and Kobayashi 1996, Burkholder et al. 2009). Aloft, on the upper half of the ridge, can be seen a compensating upslope flow (perhaps also present over the valley floor, but not seen in profiles below 100 m AGL). Thus WRF has produced a shallow drainage flow. Not evident from Fig. 18 is the fact that above 10 m there is an easterly (alongslope) component ($\overline{u}$).

b. Temperature field

Switching now to the thermal field, Fig. 19 is the potential temperature θ at 2 m AGL over domain 2 (θ has been defined with respect to a nominal sea level pressure of 1013 hPa). The rationale for displaying the pattern in θ (at fixed height AGL) is that this field would be uniform, irrespective of surface elevation, were the atmosphere neutrally stratified: in effect, viewing $\overline{\theta}$(2 m) eliminates a 'background' elevation-related temperature pattern that would otherwise potentially confound the interpretation of the effect of the drainage winds. Were an initially neutral atmosphere—i.e. one with uniform potential temperature—to slide, without surface heat exchange, over hilly terrain, uniformity of the potential temperature would be sustained: θ(2 m) would be indifferent to the local topographic elevation.

The point conveyed by Fig. 19 is that the slopes and tops are mild and the valleys are filled with colder air, as might be expected after nocturnal radiative cooling over sloping

[5] Terry's (1999) Figure 7.5 gives daily wind run for several Southland stations. For several days (5–8 July) during this relatively calm period, Gore's daily mean winds were the strongest of those reported. This may be a reflection of sustained drainage winds, escaping to the coast from the inland valleys.

[6] Katurji and Zhong (2012) used the Advanced Regional Prediction System (ARPS) to investigate drainage winds and cold air ponding in idealised two-dimensional basins. Height resolution (10 m) was comparable with that of the present study, and these authors likewise observed that the largest downslope velocity normally occurred at the lowest gridpoint, commenting that finer resolution would be needed to better resolve the profile of the drainage layer ('near-surface downslope jet').

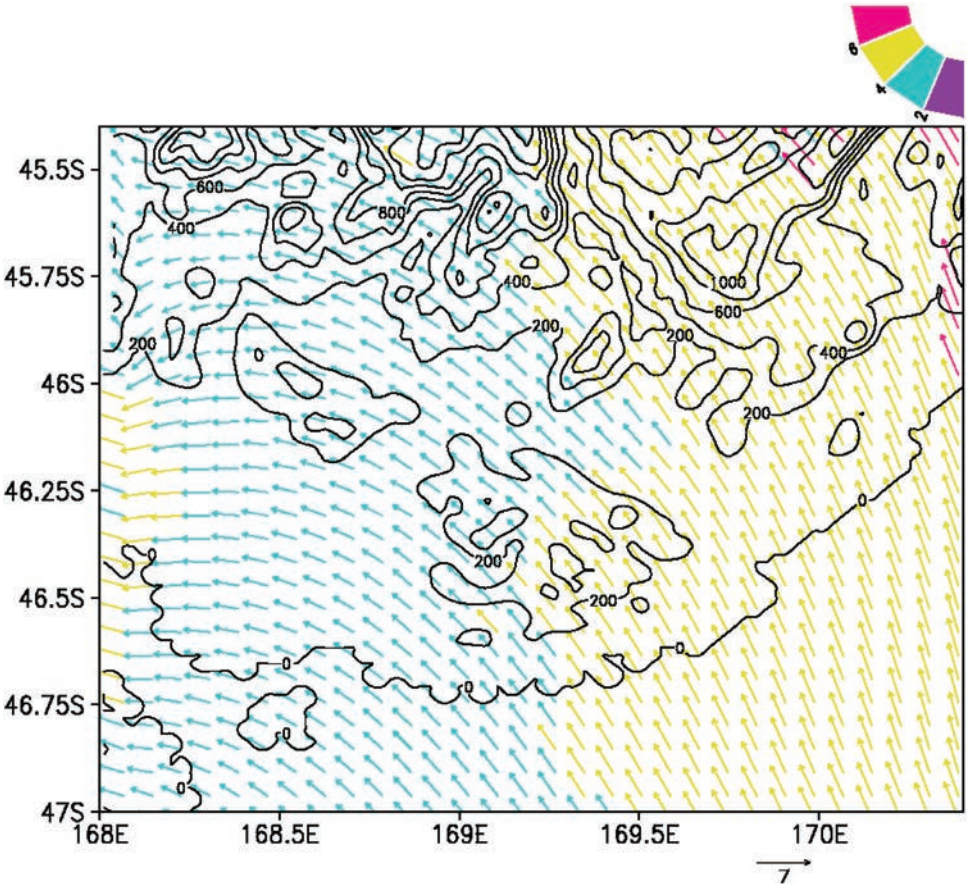

Fig. 13. WRF simulation valid at t_0 + 12 (0600 NZST, 4 July 1996). Horizontal wind vectors (scale: m s^{-1}) at the 850 hPa level over domain 1 (y-axis spans 178 km with resolution Δy = 2 km).

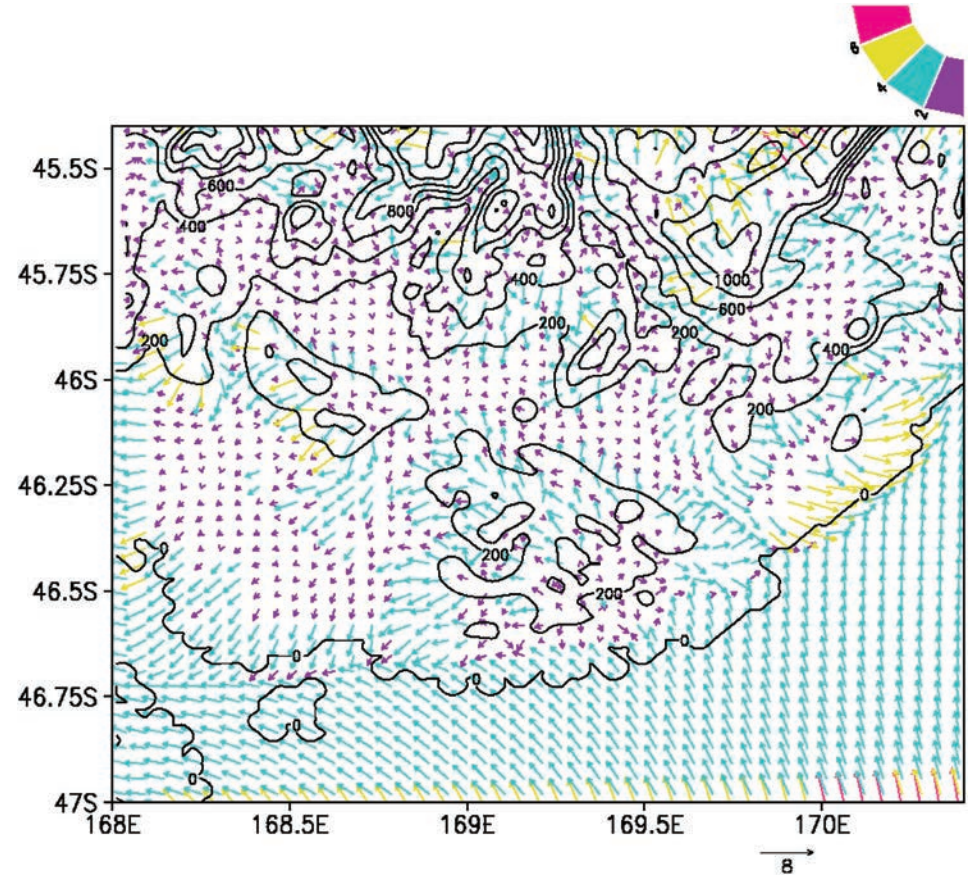

Fig. 14. WRF simulation valid at t_0 + 12 (0600 NZST, 4 July 1996). Horizontal wind vectors (scale: m s^{-1}) at 10 m AGL over domain 1 (y-axis spans 178 km with resolution Δy = 2 km). Gore AWS (46.115°, 168.887°) reported a weak northerly wind.

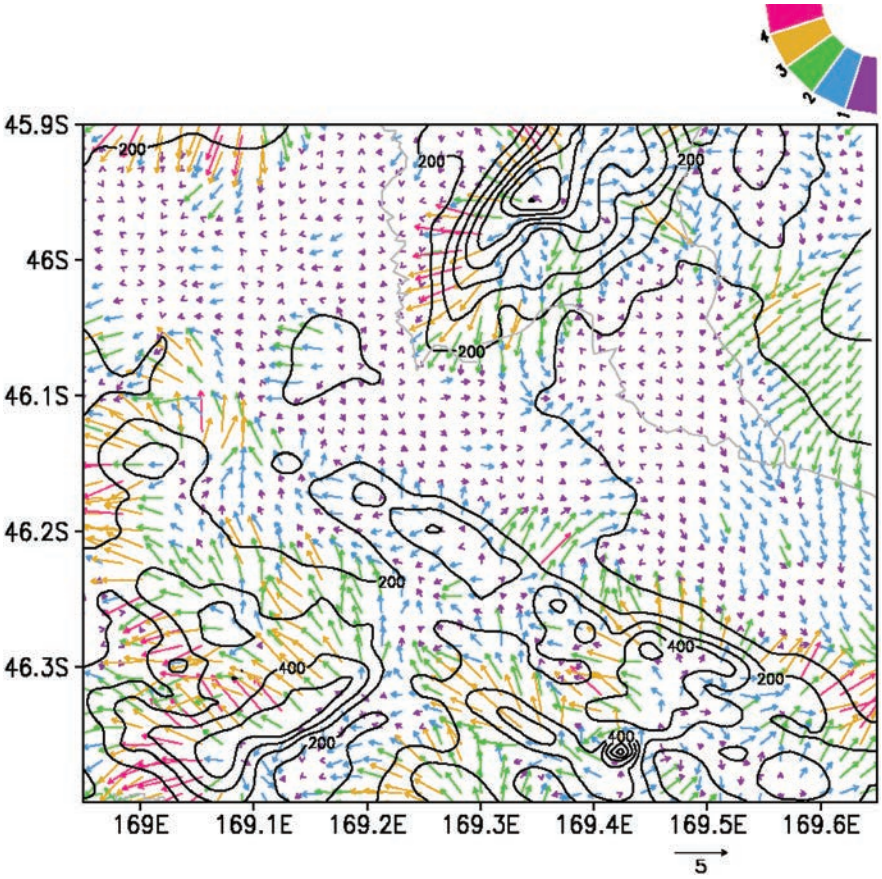

Fig. 15. WRF simulation valid at t_0 +1200 (0600 NZST 4 July 1996). Horizontal wind vectors at 10 m AGL over domain 2 (y-axis spans 55.5 km with resolution Δy = 666 m). Light grey lines denote rivers; the Pomahaka, looping around the base of the Blue Mountains (which peak near the upper centre of figure), joins the Clutha (Mata-Au) River which exits on the right of the diagram and flows to Molyneux Bay. Gore AWS (46.115°, 168.887°) reported a weak northerly wind.

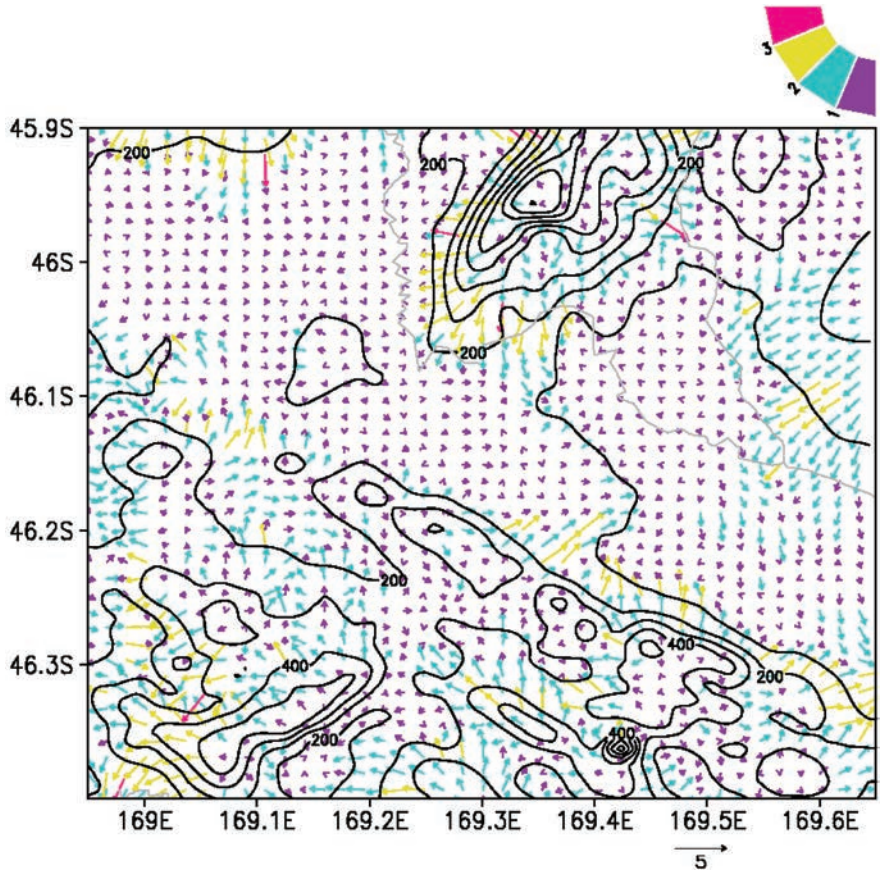

Fig. 16. WRF simulation valid at t_0 +1200 (0600 NZST 4 July 1996). The vector difference over domain 2 between the 10 m wind fields from a simulation with 59 levels and another with the (default) 45 levels.

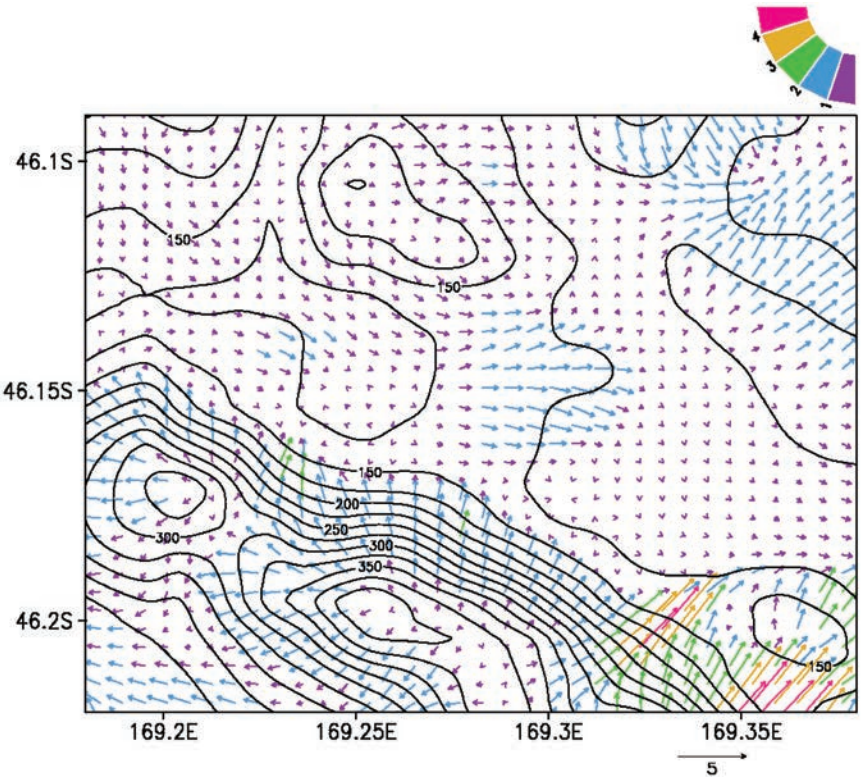

Fig. 17. WRF simulation valid at t_0 +1200 (0600 NZST 4 July 1996). Horizontal wind vectors at 10 m AGL over domain 3 (y-axis spans 14.4 km with resolution Δy = 222 m).

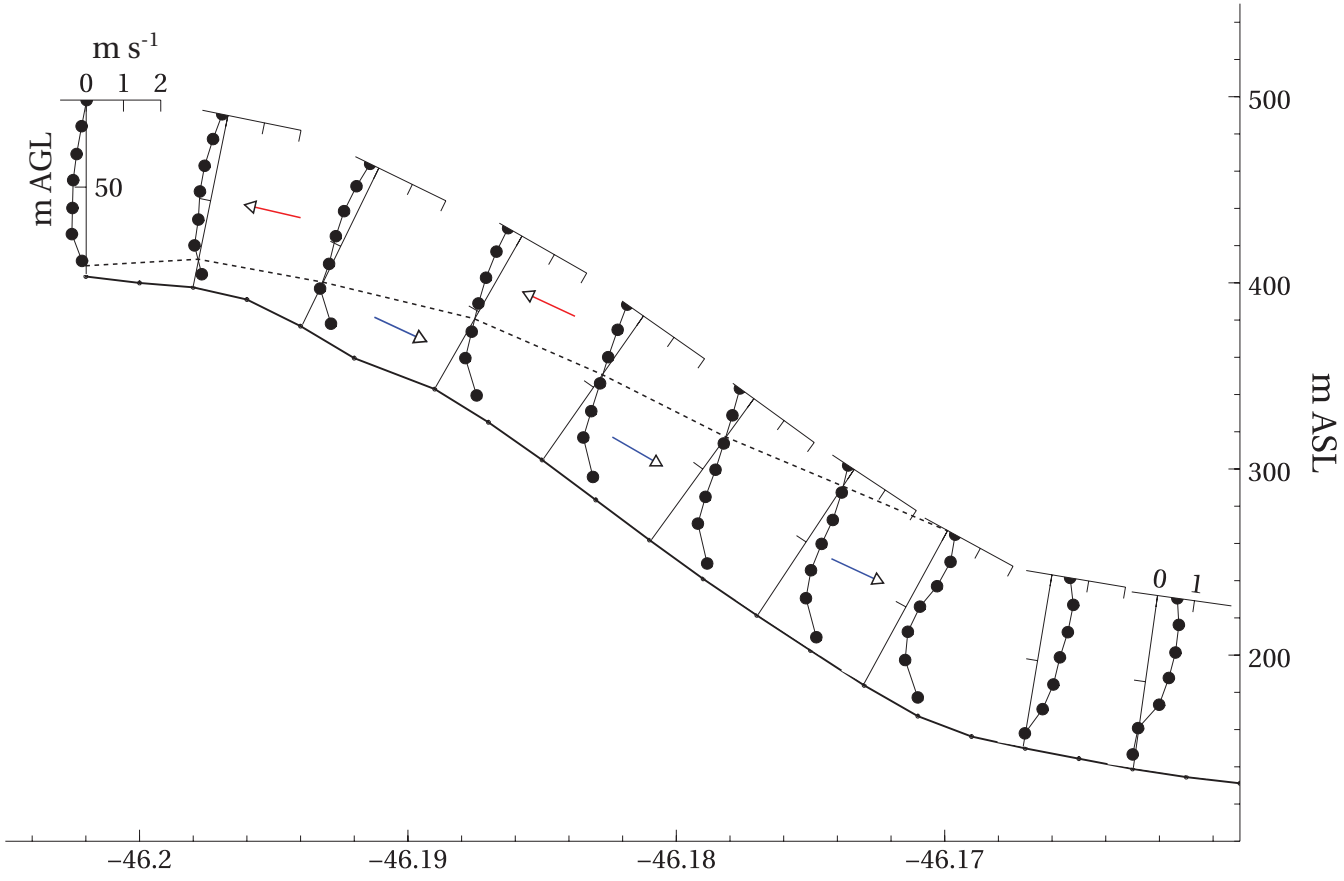

Fig. 18. WRF simulation valid at t_0 +1200 (0600 NZST 4 July 1996). Transect of the drainage layer (slope wind) down the slope south of *Strathearn,* at longitude 169.265°E where the terrain slopes north and where the mean wind at 10 m AGL is due southerly (see previous figure). Insets give a sequence of profiles of the north–south (locally up/down slope) component ($\bar{v}$), all extending to 100 m above local ground level, and all sharing the same scale for the wind speed. The dashed line separates the ground-based drainage current from a return current aloft.

Fig. 19. WRF simulation valid at t_0 +1200 (0600 NZST 4 July 1996). The field of potential temperature at 2 m AGL over domain 2.

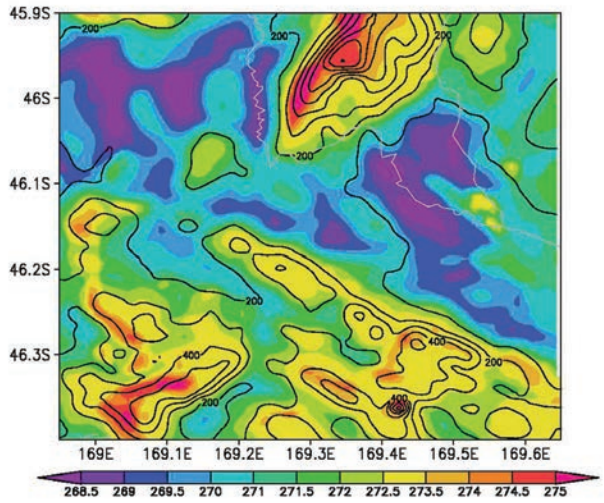

Fig. 20. WRF simulation valid at t_0 +1200 (0600 NZST 4 July 1996). The field of potential temperature at 2 m AGL, over domain 3. At the valley bottom this may be read as equating to the actual (true) temperature, implying a minimum screen-height temperature for 4 July 1996 (NZST) of about –5° C at Wairuna.

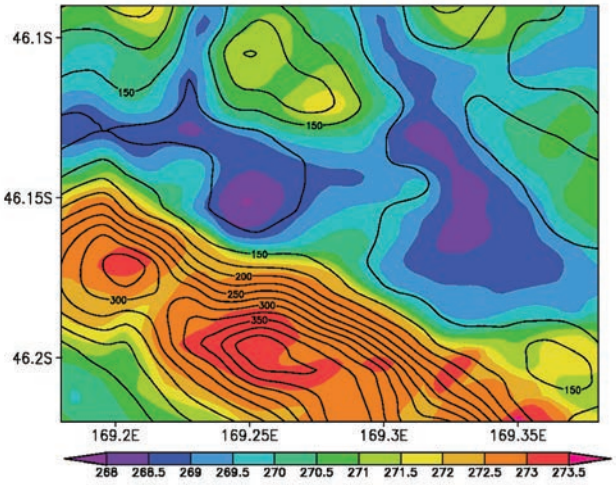

terrain. The weaker downslope winds of a low resolution run (45 levels; not shown) resulted in near ground temperatures in the Wairuna valley that were warmer by up to about 1.5 °C than those of the 59-level run (i.e. Fig. 19), with similar or larger differences elsewhere.

Finally, Fig. 20 is the field of θ(2 m) over domain 3. The coldest (potential) temperatures are just below 268 K or –5 °C, and this figure applies equally to the true temperature (in this case the true temperature slightly exceeds the potential temperature, due to the fact that the latter had been defined relative to a reference pressure of 1013 hPa whereas the WRF solution gave 1020 hPa for the surface pressure at *Strathearn* where surface elevation is about 130–135 m ASL). No local measurement is available to confirm this figure, however it does seem plausible given the observed range of minimum screen-level temperatures in the region (Table 1) with –10.5 °C in Gore and –6.5 °C at Balclutha. Temperature at grass level—or rather, on the surface of the prevailing snow cover—would have been considerably colder.

Conclusions

This paper has briefly documented some elements of the meteorology associated with extreme cold in Southern New Zealand, and has explored the capability of a contemporary mesoscale model to 'downscale' past observations (as assimilated into the standard reanalyses) and reveal mechanisms at work on the micro-scale.

The patterns given by WRF cannot be claimed to be grid independent, and (more specifically) one readily detects a dependence of the near-ground winds on the vertical resolution of the simulation. Another source of non-uniqueness is that downscaled flows differ noticeably (albeit not in their essence) depending on which of the available sets of reanalysis fields are chosen to provide the needed initial and boundary conditions. Interestingly though, notwithstanding the high spatial resolution attained on the innermost domain (domain four, resolution ~75 m, results not shown), there were found to be only a small differences between non-hydrostatic and hydrostatic runs. This is consistent with the review of Mahrt (1982), who terms as 'quasi-hydrostatic' and 'usual' the situation that the z-equation (here Eqn. 2) is hydrostatic while 'the component of the gravitational force parallel to the slope is not balanced and leads to downslope acceleration.'

Unfortunately the low density of officially documented weather observations over the region of interest prohibits evaluation of the accuracy of these downscaled meteorological fields, which do however confirm that drainage winds played an important local role in the Big Freeze (visual evidence of cold air ponding is given in the booklet by Taylor 2012) and resulted in a mesoscale drainage current venting down-valley to the coast. Overall, no element of the simulations jars with what is known of the event; and notwithstanding the perceived extremity of the cold, the meteorology behind it has no appearance of being qualitatively out of the ordinary. Repeats are to be expected.

Acknowledgments

Simulations with WRF were performed using the United States NOAA/NWS Science and Training Resource Center (STRC) Environmental Modeling System (EMS), which is supported by Dr. R.A. Rozumalski, Science and Training Resource Coordinator of the United States National Weather Service. The NCEP/DOE reanalysis (here used to provide

initial and boundary conditions for WRF simulations) was produced with the support of the U.S. National Weather Service and U.S. Department of Energy. Lorraine Johnston, of the Dunedin Public Library, provided archived weather forecasts from the Otago Daily Times.

References

Bannister, P. 2003. Are frost hardiness ratings useful predictors of frost damage in the field? A test using damage records from the severe frost in South Otago and Southland, New Zealand, July 1996. *N.Z. J. Botany, 41 (3)*, 555–69.

Brost, R. and J. Wyngaard. 1978. A model study of the stably stratified planetary boundary layer. *J. Atmos. Sci., 35*, 1427–40.

Burkholder, A., Shapiro, A. and E. Fedorovich. 2009. Katabatic flow induced by a cross-slope band of surface cooling. *Acta. Geophysica, 57*, 923–49.

Jiménez, P. and Dudhia, J. 2012. Improving the representation of resolved and unresolved topographic effects on surface wind in the WRF model. *J. Appl. Meteorol. Climatol., 51*, 300–16.

Jiménez, P. and Dudhia, J. 2013. On the ability of the WRF model to reproduce the surface wind direction over complex terrain. *J. Appl. Meteorol. Climatol., 52*, 1610–17.

Katurji, M. and Zhong, S. 2012. The influence of topography and ambient stability on the characteristics of cold-air pools: a numerical investigation. *J. Appl. Meteorol. Climatol., 51*, 1740–49.

Mahrt, L., 1982. Momentum balance of gravity flows. *J. Atmos. Sci., 39*, 2701–11.

Mori, M. and Kobayashi, T. 1996. Dynamic interaction between observed nocturnal drainage winds and a cold air lake. *J. Meteorol. Soc. Japan, 74*, 247–58.

Noh, Y., Cheon, W., Hong, S., and Raasch, S. 2003. Improvement of the K-profile model for the planetary boundary layer based on large eddy simulation data. *Boundary-Layer Meteorol., 107*, 401–27.

Rogers, R., Deng, A., Stauffer, D., Gaudet, B., Jia, Y., Soong, S.-T. and Tanrikulu, S. 2013. Application of the Weather Research and Forecasting model for air quality modeling in the San Francisco Bay area. *J. Appl. Meteorol. Climatol., 52*, 1953–73.

Santos-Alamillos, F. et al., 2013. Analysis of WRF model wind estimate sensitivity to physics parameterization choice and terrain representation in Andalusia (southern Spain). *J. Appl. Meteorol. Climatol., 52*, 1592–1608.

Shin, H. and Hong, S.-Y. 2011. Intercomparison of planetary boundary-layer parametrizations in the WRF model for a single day from cases–99. *Boundary-Layer Meteorol., 139*, 261–81.

Suselj, K. and Sood, A. 2010. Improving the Mellor-Yamada-Janjic parameterization for wind conditions in the marine planetary boundary layer. *Boundary-Layer Meteorol., 136*, 301–24.

Taylor, H., 2012. *Dinkum Cold or Disbelief*. Strathearn Taylors, 52pp, ISBN 978-0-473- 20386-3.

Terry, B., 1999. Mortality among Southland's shelterbelt trees. M.S. thesis, University of Otago, 246pp.

Troen, I. and Mahrt, L. 1986. A simple model of the atmospheric boundary layer: Sensitivity to surface evaporation. *Boundary-Layer Meteorol., 37*, 129–48.

Wood, J., 1998. The effects of an abnormally cold winter spell on southland birds. *Notornis, 45*, 126–28.

Yang, Q. et al., 2013. Evaluation of WRF-predicted near-hub-height winds and ramp events over a Pacific Northwest site with complex terrain. *J. Appl. Meteorol. Climatol., 52*, 1753–63.